Asian Journal of Chemistry; Vol. 29, No. 10 (2017), 2191-2196

ASIAN JOURNAL OF CHEMISTRY

https://doi.org/10.14233/ajchem.2017.20681

Thermal Expansion, Microhardness and Oxygen Permeation of $La_{1-x}Sr_xCo_{0.8}Fe_{0.2}O_{3+\delta}$ Membranes

A. ALIYATULMUNA[1,2], W.P. UTOMO[1], R.Y.P. BURHAN[1], H. FANSURI[1,*] and I.K. MURWANI[1,*]

[1]Department of Chemistry, Institut Teknologi Sepuluh Nopember (ITS), Kampus ITS Sukolilo, Surabaya 60111, Indonesia
[2]Department of Chemistry, Universitas Negeri Malang (UM), Jalan Semarang 5, Malang 65145, Indonesia

*Corresponding authors: Tel.: +62 31 5935208; E-mail: h.fansuri@chem.its.ac.id; irmina@chem.its.ac.id

Received: 31 March 2017; *Accepted*: 15 June 2017; *Published online*: 31 August 2017; AJC-18517

Dense ceramic membranes acting as oxygen and electron ion-conductors can be used as the catalysts for syngas production. The $La_{1-x}Sr_xCo_{0.8}Fe_{0.2}O_{3+\delta}$ (LSCF) systems were known to have a high ionic and electronic conductivity. In the application, the $La_{1-x}Sr_xCo_{0.8}Fe_{0.2}O_{3+\delta}$ membranes required low thermal expansion, microhardness and high oxygen permeation flux. The changes in the expansion, hardness, and oxygen flux of the $La_{1-x}Sr_xCo_{0.8}Fe_{0.2}O_{3+\delta}$ perovskite membranes with various strontium substitutions were studied. The magnitude of both the thermal expansion and the oxygen content of the $La_{1-x}Sr_xCo_{0.8}Fe_{0.2}O_{3+\delta}$ membranes decreased with up to 20 % strontium substitution and then increased with 30 and 40 % strontium ion substitution. Meanwhile, the hardness and shrinkage improved by various strontium ion substitutions, except with 20 % strontium. The highest oxygen flux over $La_{1-x}Sr_xCo_{0.8}Fe_{0.2}O_{3+\delta}$ ($0.0 \leq x \leq 0.4$) membranes in the surface exchange-controlled processes was found of the membrane with 30 % strontium substitution.

Keywords: Oxygen flux, Oxygen Non-stoichiometry, Shrinkage.

INTRODUCTION

Perovskite type oxides based on $LaCoO_3$ is an interesting topic, since it has the capability to conduct oxygen anions through a difference in oxygen activity between high and the low partial pressure side [1]. Material of oxygen ion conductor is used as oxygen pump in fuel cell system and also as membrane catalysts in partial oxidation reaction which produce synthesis gas and methanol [2].

To increase the transport of oxygen ion, it is necessary to substitute A and B site cations of $LaCoO_3$ perovskite oxide, such as substitution in $La_{1-x}Sr_xCo_{0.8}Fe_{0.2}O_{3+\delta}$ (LSCF). Three decades ago, Teraoka was the first researcher who observed $La_{1-x}Sr_xCo_{0.8}Fe_{0.2}O_{3+\delta}$ material. Hence forth, there is research on the properties of oxygen ion transport and its influence on the oxygen separation from the air in LSCF materials [3].

$La_{1-x}Sr_xCo_{0.8}Fe_{0.2}O_{3+\delta}$ dense membranes as the catalyst in industrial processes require low thermal expansion value, thermal stability and high oxygen permeation. The difference in thermal expansion coefficient between the air side of the membrane and the oxygen-lean side of the membrane results in the cracking of membrane in high-temperature quartz reactor [4]. The thermal expansion coefficient in the LSCF reduced along with the decreasing strontium ion substitution [5]. However, the low Sr substitution in LSCF caused the reduction of ionic conductivity [6]. The researchers observe the content of ions in LSCF's B site, the cobalt ion enhances the transport property of oxygen ion. However, it also decreases the thermal stability in reduction atmosphere. Meanwhile, iron ion increases the thermal stability and has the highest ionic conductive property as well as electronic conductive after cobalt [1].

There are many studies on $La_{1-x}Sr_xCo_{0.8}Fe_{0.2}O_{3+\delta}$ composition with a high content of both strontium and cobalt [7]. However, there is still limited information on thermal expansion and oxygen transport characteristics of LSCF membranes with low Sr and high Co contents. Hence, this research aimed to characterize the hardness, thermal expansion and oxygen flux of $La_{1x}Sr_xCo_{0.8}Fe_{0.2}O_{3+\delta}$ with 0 until 40 % Sr substitution effect for lanthanum with 10 % intervals (x = 0.0-0.4). The thermal expansion coefficient of material in the air has a similar tendency with such material thermal expansion coefficient in reducing atmosphere at various temperatures [8]. The crystal structure and thermal stability were also observed to support transport property of oxygen ion of $La_{1-x}Sr_xCo_{0.8}Fe_{0.2}O_{3+\delta}$ (x = 0.0-0.4).

EXPERIMENTAL

Powder synthesis: The perovskite materials of LSCF (x = 0.0-0.4) series were synthesized by solid state reaction method from oxide precursors. The chemicals used in the preparation were La_2O_3 (Merck, 99.5 %), Co_3O_4

(Aldrich, 99.5%), Fe_2O_3 (Merck, 97 %) and $Sr(NO_3)_2$ (Merck, 99.0 %).

The precursors with particular stoichiometric comparisons were mixed and put into ball mills with an amount of methanol for 24 h to be then drained at 60 °C. After drained, the precursors were then calcined in the furnace at 1000 °C for 2 h. The calcination process was repeated one more time to refine the formation of perovskite.

Characterizations: The thermal characteristics of perovskite oxide powder were characterized by using TGA/DSC. The utilized TGA/DSC method was adopted from Wang *et al.* [9]. The method was initiated with the sintering process on the powder material from room temperature up to 950 °C with the increasing temperature rate of 100 °C/min. The materials were left at the temperature of 950 °C for 60 min. Subsequently, the temperature was cooled down from 950 °C to room temperature. Then, the materials were left at the room temperature for 10 min. Next, the powder materials were sintered one more time up to the temperature of 1100 °C with 10 °C/min sintering rate in the flow of 5 %H_2/Ar and with the flow rate of 20 mL/min. The materials were left for 180 min after reaching 1100 °C.

Subsequently, the phase compositions of the synthesized perovskite oxides were then determined *via* X-ray diffraction. The diffraction characterization was performed at a 2θ starting from 30° until 60° with the interval of 0.02° and the speed of 6° min^{-1}. The utilized X-ray is $K_{\alpha 1}$ radiation sourced from Cu with the wavelength (λ) of 1.54056 Å.

The synthesized perovskite oxides of LSCF were then pressed to be disks and sintered at 1100 °C for 8 h. The characterization of hardness of disk shaped membranes was performed in HM-200-Mitutoyo series of an Micro Vickers Hardness. The load given to the material was 1 N with the indentation period of 30 min. The characterization of membrane hardness was conducted in 7 membrane points.

The scanning electron microscopy (SEM) was conducted to observe the surface morphology of the membranes using ZEISS EVO MA 10. The thermal expansion coefficient (TEC) was characterized using Thermal Mechanical Analyzer (TMA) (Mettler Toledo, Switzerland). The Thermal Mechanical Analyzer was used at the temperature of 200 up to 1100 °C on the temperature increasing rate of 20 °C/min.

The oxygen flux measurements utilized silver paste as the adhesive between the membrane sample and the quartz tube. They were carried out at 550 to 950 °C with the temperature increasing rate of 100 °C min. The oxygen acted as the feed gas on the flow rate of 150 mL/min. High purity helium was flown on the other side of the membrane on the flow rate of 30 mL/min. The flow rate was controlled by mass flow controller (MFC).. The gas chromatography complemented with 13X molecular sieve column was then connected (inline) on the gas exit. Subsequently, the oxygen flux was measured with eqn. 1:

$$J_{O_2} = \left(\%O_2 - \left(\frac{21}{79} \right) \%N_2 \right) \cdot \frac{F}{A} \quad (1)$$

where J_{O_2} was the oxygen flux (mL min^{-1} cm^{-2}), F was the sweep gas flow rate (mL min^{-1}) and A was the membrane area (cm^2). A = 0.44 cm^2 [10].

RESULTS AND DISCUSSION

Weight loss of $La_{1-x}Sr_xCo_{0.8}Fe_{0.2}O_{3\pm\delta}$ through TGA curve The weight changes of $La_{1-x}Sr_xCo_{0.8}Fe_{0.2}O_{3\pm\delta}$ (x = 0.0-0.4) samples during the heat process from 200 °C until 1100 °C were analyzed through the TGA curve in the hydrogen atmosphere (Fig. 1). The weight change curves of the x = 0.1 sample and x = 0.2 sample and the x = 0.3 sample and x = 0.4 sample tend to be almost similar. There are no weight loss on the x = 0.1 sample and x = 0.2 sample at the temperature range of 560-640 °C. Whereas, there are weight loss caused by the $SrCO_3$ decomposition on x = 0.3 sample and x = 0.4 sample. The weight losses of the $La_{1-x}Sr_xCo_{0.8}Fe_{0.2}O_{3+\delta}$ (x = 0-0.4) samples are usable in the determination of contents of both oxygen anions and B site cations of $La_{1x}Sr_xCo_{0.8}Fe_{0.2}O_{3+\delta}$ with regard to a following decomposition reaction [11]:

$$La_{1-x}Sr_xCo_{0.8}Fe_{0.2}O_{3+\delta} \xrightarrow{5\% H_2} (1-x)/2La_2O_3 + xSrO + 0.8Co + 0.2\,Fe + ((3+\delta) - (1-x).1.5 - x).0.5O_2$$

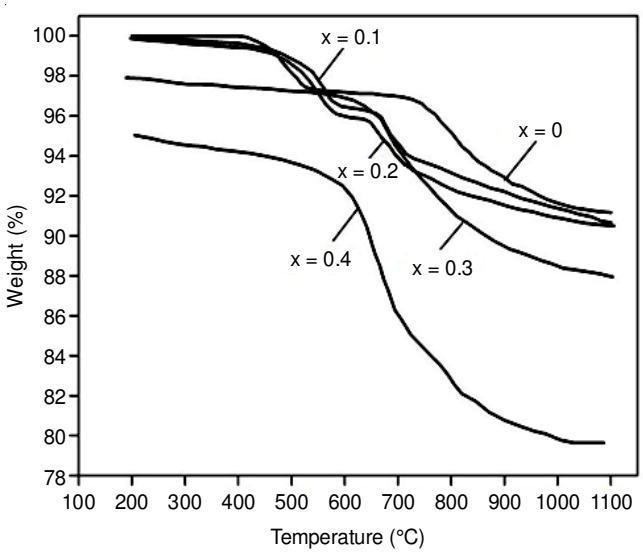

Fig. 1. Temperature dependence of the weight loss of $La_{1-x}Sr_xCo_{0.8}Fe_{0.2}O_{3+\delta}$ membranes in 5 % H_2

Table-1 shows that the samples with the higher contents of oxygen result in the larger weight losses. The x = 0. 4 sample contains more Co^{3+} and Fe^{4+} than the x = 0.3 sample.

Besides substitution of Sr^{2+} that is higher, the x = 0.4 sample contains more oxygen anions than the x = 0.3 sample. The high oxidation state (Co^{3+} and Fe^{4+}) of x = 0.4 sample be important in order to maintain the electroneutrality of the sample. Meanwhile, the x = 0.3 and x = 0.4 samples have higher Co^{2+} and Fe^{3+} content than x = 0.1 and x = 0.2 samples. The formations of $SrCO_3$ on x = 0.3 and x = 0.4 samples are balanced by a number of B site cations of $La_{1-x}Sr_xCo_{0.8}Fe_{0.2}O_{3+\delta}$ with low oxidation state (Co^{2+} and Fe^{3+}).

Crystal structure of $La_{1-x}Sr_xCo_{0.8}Fe_{0.2}O_{3+\delta}$: The crystal phases of the powder material of $La_{1-x}Sr_xCo_{0.8}Fe_{0.2}O_{3+d}$ (x = 0-0.4) were identified by using XRD (Fig. 2). All samples have perovskite phase with the $SrCO_3$ phase (PDF No. 71-2393) identified in sample with 30 % and 40 % Sr substitution (x = 0.3 and x = 0.4) for La. The formations of strontium carbonate result from some Sr which get out of the $La_{1-x}Sr_xCo_{0.8}Fe_{0.2}O_{3+\delta}$

TABLE-1
WEIGHT LOSSES OF VARIOUS Sr SUBSTITUTIONS IN 5 % H_2

$La_{1-x}Sr_xCo_{0.8}Fe_{0.2}O_{3\pm\delta}$ samples	Weight loss of samples (%)	Oxygen content (3 + δ)	Cation contents at B site over $La_{1-x}Sr_xCo_{0.8}Fe_{0.2}O_{3+\delta}$ (%)			
			Co^{2+}/Co^{3+}		Fe^{3+}/Fe^{4+}	
			Co^{2+}	Co^{3+}	Fe^{3+}	Fe^{4+}
x = 0.0	8.52	3.06	N/A	N/A	100	0
x = 0.1	8.51	2.68	45.3	54.7	53.4	46.6
x = 0.2	8.36	2.63	50.0	50.0	39.7	60.3
x = 0.3	8.73	3.07	95.2	4.8	97.3	2.7
x = 0.4	12.07	3.15	90.9	9.1	85.4	14.5

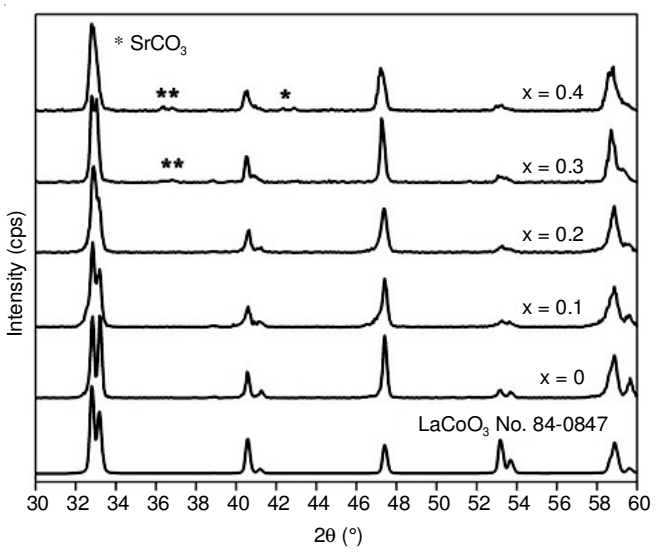

Fig. 2. XRD pattern of $La_{1-x}Sr_xCo_{0.8}Fe_{0.2}O_{3+\delta}$ samples

lattice and reacted with the CO and CO_2 in the air [12]. All $La_{1-x}Sr_xCo_{0.8}Fe_{0.2}O_{3+\delta}$ samples possess a rhombohedral structure, similar to structure of the $LaCoO_3$ parent (PDF No. 84-0847). Both edge length (a) and volume of unit cell increase with increasing of Sr substitution (Table-2). The rhombohedral structure approaches cubic structure when unit cell angle of x = 0.4 is smallest and its peak (2θ ≈ 32.8-33.2) is sharp single (2θ ≈ 32.8-33.2) [13].

TABLE-2
LATTICE PARAMETERS OF $La_{1-x}Sr_xCo_{0.8}Fe_{0.2}O_{3+\delta}$

Sample	x	a (nm)	Unit cell volume $(nm^3)^a$	α (°)
$LaCo_{0.8}Fe_{0.2}O_3$	0.0	0.5379	0.1118	60.72
$La_{0.9}Sr_{0.1}Co_{0.8}Fe_{0.2}O_3$	0.1	0.5386	0.1121	60.66
$La_{0.8}Sr_{0.2}Co_{0.8}Fe_{0.2}O$	0.2	0.5401	0.1128	60.54
$La_{0.7}Sr_{0.3}Co_{0.8}Fe_{0.2}O_3$	0.3	0.5408	0.1131	60.48
$La_{0.6}Sr_{0.4}Co_{0.8}Fe_{0.2}O_3$	0.4	0.5412	0.1133	60.45

[a]Unit cell volumes were calculated by the equation:
$V = a^3\sqrt{1-3(\cos\propto)^2+2(\cos\propto)^3}$ [Ref. 12]

Discussion about the chemical expansion [14] of samples with respect to data from both TGA and XRD is as follows:

The chemical expansion is defined with the eqn. 2:

$$\varepsilon = \frac{(a_x - a_0)}{a_0} \quad (2)$$

where a_x is unit cell edge of $La_{1-x}Sr_xCo_{0.8}Fe_{0.2}O_{3+\delta}$ for Sr substitution from 10 up to 40 % (x = 0.1-0.4) and a_0 is unit cell edge when x = 0.0 [15]. The chemical expansions of $La_{1-x}Sr_xCo_{0.8}Fe_{0.2}O_{3+\delta}$ increased sharply with Sr substitution increasing to x = 0.2. However slight increasing of chemical expansions is observed for the sample of x = 0.3 until x = 0.4 (Fig. 3). It is possible since the maximum Sr which could substitute La on $La_{1-x}Sr_xCo_{0.8}Fe_{0.2}O_{3\pm\delta}$ lattice is less than 30 % (x < 0.3).

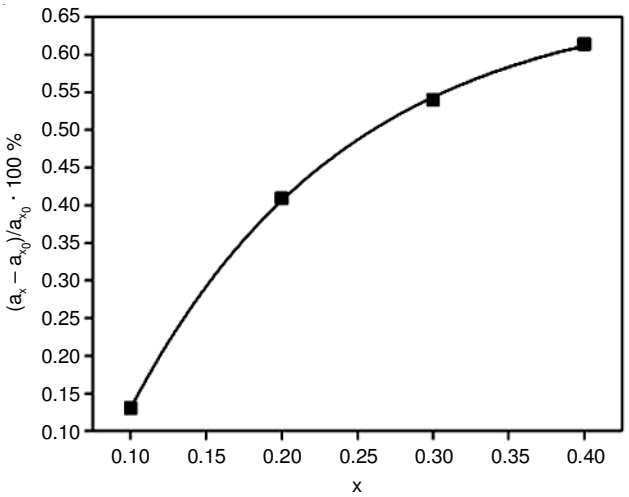

Fig. 3. Influences of Sr substitution on chemical expansion

The x = 0.4 sample has higher lattice parameters and larger chemical expansion than the x = 0.3 sample, even though the differences are slight. It is because the x = 0.4 sample contains higher oxidation anions, Co^{3+} and Fe^{3+} compared with the x = 0.3 sample (Table-1).

Besides larger radius of Sr^{2+} than that of La^{3+} ($r_{Sr^{2+}} = 0.158$ nm and $r_{La^{3+}} = 0.150$ nm), the distance between ions in $La_{1-x}Sr_xCo_{0.8}Fe_{0.2}O_{3+\delta}$ also contributes towards the increase of the lattice parameters and chemical expansion. The excess oxygen ions of x = 0.4 sample increase the repulsion between oxygen anions so that the distance between the oxygen anions in the lattice of x = 0.4 sample increase and the cations radius on A site became larger [16]. Additionally, the repulsion between La^{3+} and cations in B site with high oxidation state, *i.e.* Co^{3+} and Fe^{4+}, also increase the La^{3+}-(Co^{3+}, Fe^{4+}) distance on x = 0.4 sample.

Thermal expansion coefficient (TEC): The thermal expansion coefficient of all $La_{1-x}Sr_xCo_{0.8}Fe_{0.2}O_{3+\delta}$ membranes started to increase at the temperature of 200 °C up to 850 °C and then reduced up to 1100 °C (Fig. 4). The increase of thermal expansion coefficient by temperature was caused by the formation of larger particles [17]. The densification and formation of particles started at the temperature of 850 °C and leads to the contraction of $La_{1-x}Sr_xCo_{0.8}Fe_{0.2}O_{3+\delta}$ lattice [18].

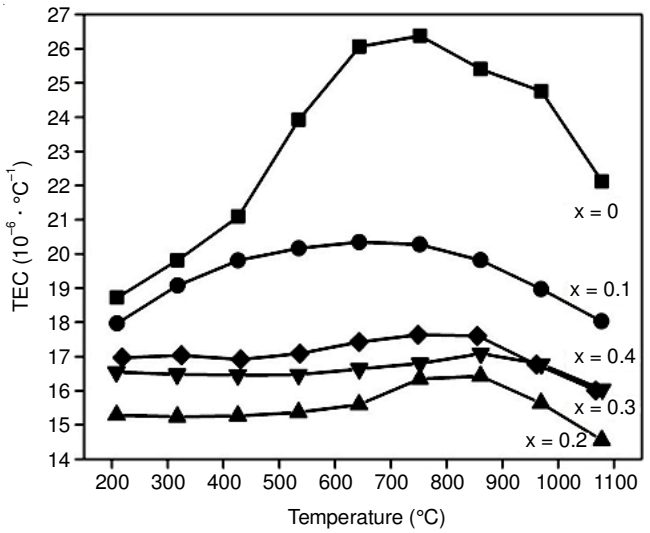

Fig. 4. Temperature probes of the thermal expansion coefficient in air for $La_{1x}Sr_xCo_{0.8}Fe_{0.2}O_{3+\delta}$ samples

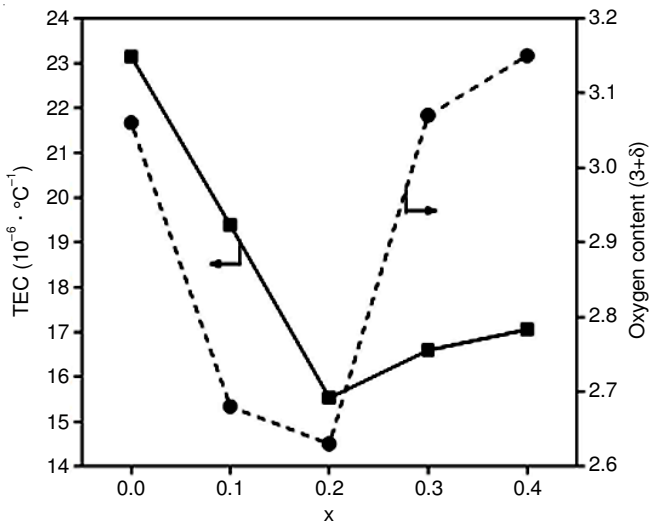

Fig. 5. Correlation between the thermal expansion coefficient,the oxygen content and the Sr substitution for $La_{1-x}Sr_xCo_{0.8}Fe_{0.2}O_{3+\delta}$ samples

The average TEC and the oxygen content in $La_{1-x}Sr_xCo_{0.8}Fe_{0.2}O_{3+\delta}$ have a similar curve (Fig. 5). The x = 0.2 sample has both the smallest oxygen stoichiometry and the highest Fe^{4+} content (Table 1). The oxygen losses lead the decrease in the coordination number of A site metal ions so that the radii of A site metal ions in $La_{1-x}Sr_xCo_{0.8}Fe_{0.2}O_{3\pm\delta}$ are also decreased [16]. The small radius of metal ion in A site and the shortened Fe^{4+}-O^{2-} distance result in the declined TEC. In the contrary, excess oxygen in x = 0.3 and x = 0.4 samples increase the TEC.

For the sample, x = 0.1, the highest content of La^{3+} results in a high level of TEC. This is due to the longer distance of La^{3+}-B-site ion than that of Sr^{2+}-B-site ion [19].

Surface morphology of membrane: The membranes with the largest Sr content, namely 40 % (x = 0.4) showed dense microstructure without obvious pores (Fig. 6). The Sr metal has the lowest melting point among other elements that compose the $La_{1-x}Sr_xCo_{0.8}Fe_{0.2}O_{3+\delta}$ compound [20]. It allows the particles in the compoundto weld easily and then formed a large particle [17]. Besides the high densification, the x = 0.4 membrane also has the largest shrinkage percentage and hardness (Fig. 7).

Different with the x = 0.4 membrane, the membranes without strontium do not experience densification but coarsening so that not only the grains but also pore sizes of the x = 0.0 membrane are large. Meanwhile, the low densification of x = 0.0 membrane is conforming to the low percentage of shrinkage and hardness of x = 0.0 membrane. Such findings support the research conducted by Tan *et al.* [21] on $Ba_{0.8}Sr_{0.2}Co_{0.8}Fe_{0.2}O_{3-\delta}$ membrane [21]. The shrinkage increases with the formation of void spaces within the lattice structure as a result of the ion substitution

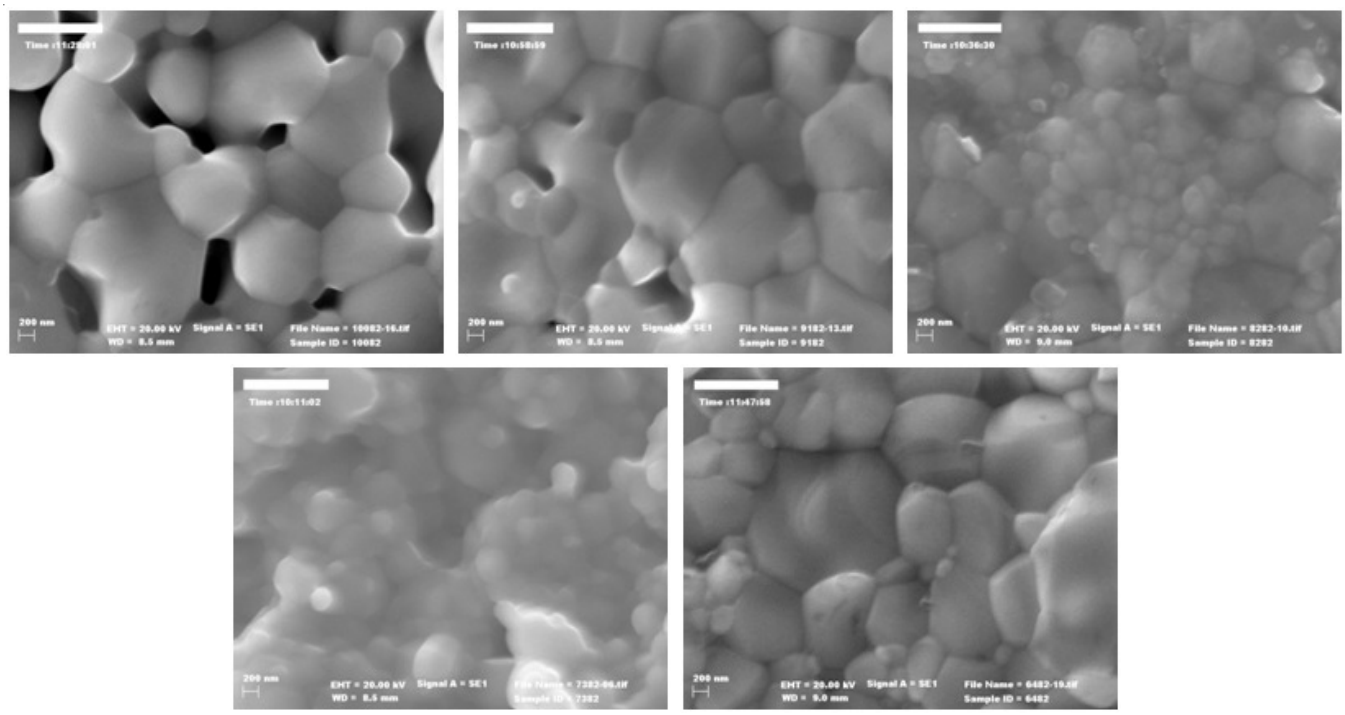

Fig. 6. SEM images of $La_{1-x}Sr_xCo_{0.8}Fe_{0.2}O_{3+\delta}$

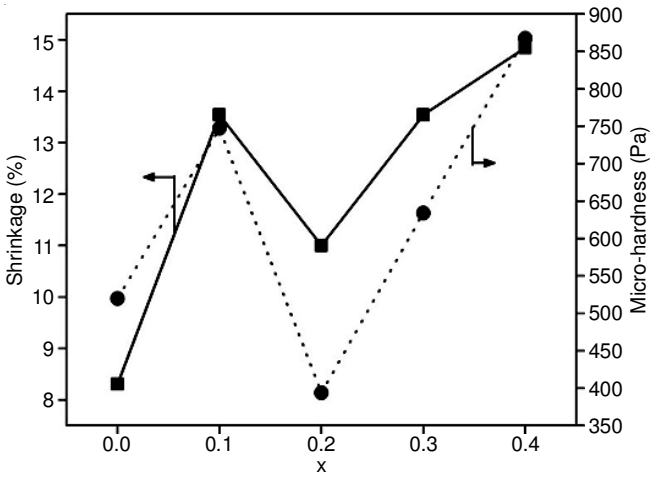

Fig. 7. Correlation between shrinkage, microhardness and Sr substitution for $La_{1-x}Sr_xCo_{0.8}Fe_{0.2}O_{3+\delta}$ membranes

with a larger radius, namely Sr^{2+}, to the ion with a smaller radius *i.e.* La^{3+} [22].

Oxygen permeation flux: The oxygen flux measurements were conducted successfully towards the x = 0.1, 0.3, and 0.4 membranes. Those membranes have a higher percentage of shrinkage and hardness compared with x = 0.0 and 0.2 membranes. The low hardness causes the x = 0.0 and x = 0.2 membranes to crack when adhered to the quartz reactor for the flux test. The highest until the lowest oxygen flux are produced by x = 0.3; 0.1 and 0.4 membranes respectively (Fig. 8). The x = 0.3 membrane have the highest oxygen flux since it is a membrane with low TEC and large grain boundary area (small-sized grains). The low TEC increases the membrane resistance towards the stress from the gradient of the oxygen partial pressure on both sides of the membranes during the oxygen flux measurements. Meanwhile, the grain boundaries acted as diffusivity paths of the oxygen. An oxygen exchange process occurred especially on the surface of the membranes (surface exchange-controlled processes) require small-sized grains (a lot of grain boundaries) so that it create large oxygen flux on the membranes [23].

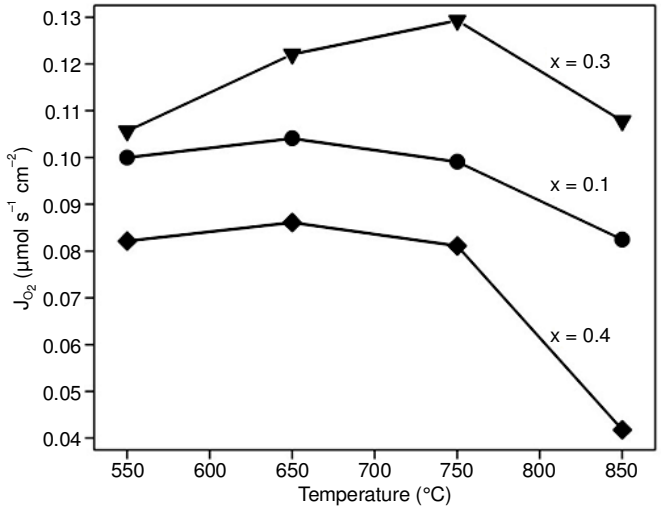

Fig. 8. Oxygen fluxes through $La_{1-x}Sr_xCo_{0.8}Fe_{0.2}O_{3+\delta}$ membranes in function of the temperature

The x = 0.1 membrane has less grain boundaries (large-sized grains) compared with the x = 0.4 membrane but the x = 0.1 membrane results in higher oxygen flux. It is made possible since the x = 0.1 sample has a higher lattice free volume than the x = 0.4 sample. The highest until the lowest lattice free volumes are respectively found in the samples of x = 0.1 (12 nm^3), 0.3 (11.8 nm^3) and 0.4 (11.5 nm^3). The reduction of lattice free volume on the x = 0.3 and x = 0.4 samples result from the samples which contain excess oxygen. According to Tan *et al.* [24], the increasing lattice free volume improves the oxygen ion transfer. The grain boundary area and then the lattice free volume mostly influence the oxygen flux in $La_{1-x}Sr_xCo_{0.8}Fe_{0.2}O_{3+\delta}$ membrane.

Conclusion

The dense ceramic membranes of $La_{1-x}Sr_xCo_{0.8}Fe_{0.2}O_{3+\delta}$ ($0.0 \leq x \leq 0.4$) had been successfully produced from the $La_{1-x}Sr_xCo_{0.8}Fe_{0.2}O_{3+\delta}$ powders which were synthesized through the means of solid state reaction method. Such membranes were characterized by using XRD, thermal gravimetric analysis, hardness, thermal expansion and oxygen flux measurement. The strontium carbonate was formed by the substitutions of 30 and 40 % strontium to lanthanum, and it affected the thermal expansion and oxygen stoichiometry. The increasing lattice parameter of $La_{1-x}Sr_xCo_{0.8}Fe_{0.2}O_{3+\delta}$ with the Sr substitution is impacted by the Sr^{2+} ion radius which is higher than that of the La^{3+} ion. Curve of thermal expansion has a similar trend to that of oxygen content value. In the oxygen flux measurement from $La_{1x}Sr_xCo_{0.8}Fe_{0.2}O_{3+\delta}$ membrane, the oxygen ion transport is primarily influenced by the grain boundary and then by the free volume of lattice.

ACKNOWLEDGEMENTS

This work was supported by the Doctoral Research Grants and the STRANAS Research Grant. Thanks are also due to the Laboratory of Energy at LPPM ITS and the Laboratory of Materials and Energy of Chemistry Department ITS, Institut Teknologi Sepuluh for providing the research facilities.

REFERENCES

1. A.F. Sammells and M.V. Mundschau, Nonporous Inorganic Membranes for Chemical Processing, John Wiley & Sons, Weinheim, Chap. 6, p. 173 (2006).
2. P.J. Gellings and H.J. Bouwmeester, Handbook of Solid State Electrochemistry, CRC Press, Inc., Chap. 14 (1997).
3. K. Li, Ceramic Membranes for Separation and Reaction, John Wiley & Sons Ltd., Chap. 6, p, 176 (2007).
4. S. Pei, M.S. Kleefisch, T.P. Kobylinski, J. Faber, C.A. Udovich, V. Zhang-McCoy, B. Dabrowski, U. Balachandran, R.L. Mieville and R.B. Poeppel, *Catal. Lett.*, **30**, 201 (1995); https://doi.org/10.1007/BF00813686.
5. A. Vivet, P.M. Geffroy, T. Chartier, P. Del Gallo and N. Richet, *J. Membr. Sci.*, **372**, 373 (2011); https://doi.org/10.1016/j.memsci.2011.02.021.
6. S.J. Skinner, *Int. J. Inorg. Mater.*, **3**, 113 (2001); https://doi.org/10.1016/S1466-6049(01)00004-6.
7. L.-W. Tai, M.M. Nasrallah, H.U. Anderson, D.M. Sparlin and S.R. Sehlin, *Solid State Ion.*, **76**, 259 (1995); https://doi.org/10.1016/0167-2738(94)00244-M.
8. E. Juste, A. Julian, G. Etchegoyen, P.M. Geffroy, T. Chartier, N. Richet and P. Del Gallo, *J. Membr. Sci.*, **319**, 185 (2008); https://doi.org/10.1016/j.memsci.2008.03.034.

9. H. Wang, Y. Cong and W. Yang, *J. Membr. Sci.*, **210**, 259 (2002); https://doi.org/10.1016/S0376-7388(02)00361-7.
10. C. Zhang, Z. Xu, X. Chang, Z. Zhang and W. Jin, *J. Membr. Sci.*, **299**, 261 (2007); https://doi.org/10.1016/j.memsci.2007.05.001.
11. S. Hashimoto, Y. Fukuda, M. Kuhn, K. Sato, K. Yashiro and J. Mizusaki, *Solid State Ion.*, **181**, 1713 (2010); https://doi.org/10.1016/j.ssi.2010.09.024.
12. N. Li, A. Boréave, J.P. Deloume and F. Gaillard, *Solid State Ion.*, **179**, 1396 (2008); https://doi.org/10.1016/j.ssi.2008.01.060.
13. J.N. Kuhn and U.S. Ozkan, *Catal. Lett.*, **121**, 179 (2008); https://doi.org/10.1007/s10562-007-9364-6.
14. Crystal Geometry Equations for XRD. https://noppa.oulu.fi/noppa/kurssi/521104p/materiaali/521104P_kaavoja_eri_hilatyypeille_ja_ kidejarjestelmille.
15. D. Marrocchelli, S.R. Bishop, H.L. Tuller and B. Yildiz, *Adv. Funct. Mater.*, **22**, 1958 (2012); https://doi.org/10.1002/adfm.201102648.
16. P. Zeng, Z. Chen, W. Zhou, H. Gu, Z. Shao and S. Liu, *J. Membr. Sci.*, **291**, 148 (2007); https://doi.org/10.1016/j.memsci.2007.01.003.
17. P. Boch and J.-C. Nièpce, Ceramic Materials: Processes, Properties, and Applications, John Wiley & Sons, Chap. 3, p. 61 (2010).
18. C. Perego and P. Villa, *Catal. Today*, **34**, 281 (1997); https://doi.org/10.1016/S0920-5861(96)00055-7.
19. H. Hayashi, M. Watanabe, M. Ohuchida, H. Inaba, Y. Hiei, T. Yamamoto and M. Mori, *Solid State Ion.*, **144**, 301 (2001); https://doi.org/10.1016/S0167-2738(01)00986-9.
20. W. Jin, S. Li, P. Huang, N. Xu, J. Shi and Y.S. Lin, *J. Membr. Sci.*, **166**, 13 (2000); https://doi.org/10.1016/S0376-7388(99)00245-8.
21. L. Tan, X. Gu, L. Yang, L. Zhang, C. Wang and N. Xu, *Sep. Purif. Technol.*, **32**, 307 (2003); https://doi.org/10.1016/S1383-5866(03)00047-9.
22. M.W. Barsoum, Fundamentals of Ceramics, IOP Publishing Ltd., Chap. 10, p. 307 (2003).
23. X. Tan, Z. Wang and K. Li, *Ind. Eng. Chem. Res.*, **49**, 2895 (2010); https://doi.org/10.1021/ie901403u.
24. L. Tan, L. Yang, X. Gu, W. Jin, L. Zhang and N. Xu, *J. Membr. Sci.*, **230**, 21 (2004); https://doi.org/10.1016/j.memsci.2003.10.019.